SUPPLEMENTARY

EMPIRICAL DATA COLLECTION AND ANALYSIS

To provide insight into the parameter space that influences the development of floodplain channels, we compiled a data set for Indiana, USA that includes the mapped floodplain extent, width, slope (David et al., 2017), upstream drainage area (Horizon Systems, 2016), streamflow gage data from the US Geological Survey (USGS), and a statewide 1.5 m resolution light detection and ranging (LiDAR) derived digital elevation model (DEM) (OpenTopography, 2013).

Floodplain mapping was performed in ESRI ArcGIS, by demarcating the lowest elevation floodplain surface for rivers greater than 20 m wide and without suburban or urban development. Floodplains were discretized into 5 km bins and classified as channelized (n=184) or not (n=838) if they passed a given channel density threshold (David et al., 2017). Characteristic floodplain channel density for each mapped floodplain was determined by taking a series of cross-sections down each floodplain segment and counting the number of channels. Floodplains were considered channelized if they had two or more channels outside of the meander belt. We only counted channels outside of the meander belt to avoid potential analysis of long wavelength chute channels or old abandoned river segments.

Mapped floodplain segments coupled with geometric centerlines for each floodplain were used to compute floodplain slope (S) and average floodplain width (W). Geometric centerlines were produced by computing Thiessen polygons along the polygon vertices and extracting the contiguous portions (Smith and Cromley, 2012; David et al., 2017). Floodplain slope was computed by differencing the elevation at the upstream and downstream ends of the floodplain

centerline and dividing by the length of the centerline. Average floodplain width was measured by dividing the mapped floodplain area by the length of the floodplain centerline (David et al., 2017). Upstream drainage area data were obtained from the NHDPlusV2 dataset and appended to mapped floodplain segments by joining the largest drainage area value that intersected the floodplain segment.

To use our empirical dataset to constrain numerical modeling experiments, it was necessary to convert our drainage area for every floodplain bin to water discharge. However, it is an interesting question as to what flow recurrence interval has the strongest influence on floodplain morphodynamics. To address this question, we analyzed the geomorphic work at all USGS stream gages that intersected our mapped floodplains (n=35). An analysis of geomorphic work explores when the most work is done on a landscape by looking at the frequency and magnitude of events (Wolman and Miller, 1960). We computed the magnitude of an event using unit stream power (Eqn .1)

$$\omega = \frac{\rho g Q S}{W} \qquad \text{Eqn. 1}$$

where, ω=unit stream power (W m^{-2}), ρ=density of water (kg m^{-3}), g= acceleration due to gravity (m s^{-2}), Q= flood discharge (m^3 s^{-1}), S = floodplain slope, and W =floodplain width (Bull, 1979). Unit stream power relates fluid flow to sediment transport and is important for floodplain erosion and deposition (Nanson and Croke, 1992). We computed unit stream power across a range of discharges from a 1 to 50 year flood using a Weibull plotting positon formula. Geomorphic work was solved for by dividing unit stream power by the recurrence interval used to calculate Q in equation 1. We found that peak geomorphic work on floodplains typically occurred between a 3 and 8 year flood (Supplementary Fig. 4), suggesting that a floodplain's ability to sculpt

topography should be highest then. Hence, for computing discharges at stream gages we chose to use a 5 year flood for our calculation.

To convert upstream drainage area to discharge for each mapped polygon, we developed a scaling relationship between drainage area and 5 year flood discharge. To accomplish this we computed the 5-year flood discharge (Q_5) using a Weibull plotting position formula for all USGS stream gages that coincided with our drainage area data and that contained at least 20 years of peak stream flow data (n=97). We chose to use a threshold of 20 years to ensure each gage had experienced multiple 5-year flooding events. Using the computed 5 year flood discharge and drainage area, we performed a power law regression and found a relationship of between Q_5 (m^3/s) and A (m^3) of the form $Q_5 = 0.000012 \times A^{0.8029}$ (Supplementary Fig. 5). This relationship was used to convert each floodplain's upstream drainage area into a 5-year flood discharge. To remove floodplain width, we normalized the computed discharge by the average floodplain width to compute a 5-year specific discharge. The specific discharge was used to guide our choices in boundary conditions for the numerical modeling experiments. Additionally, we tested the sensitivity of our results from our empirical datasets against our choice of using the 5 year flood and found that the distribution of points do not change among different recurrence intervals, where channelized floodplains always clustered at low specific discharges (Supplementary Fig. 6).

DETAILED NUMERICAL MODEL DESCRIPTION

Numerical modeling simulations were conducted using Delft3D (https://oss.deltares.nl/web/delft3d; Lesser et al., 2004), which computes the Saint Venant equations and couples fluid flow to sediment transport. Delft3D separates sediment into non-

cohesive (greater than 64 μm) and cohesive sediment (less than 64 μm). The non-cohesive and cohesive sediment transport were simulated using the Meyer-Peter Muller equation and the Partheniades-Krone formulation, respectively.

The computational grid has square cells with a nominal spacing of 15 m in the floodplain. Additionally, all cells within ~100 m of the trench were refined to have a nominal spacing of 5 m parallel to the trench and 15 m perpendicular to the trench (Supplementary Fig. 1). This allowed for detailed observations as headcuts initially developed. Sensitivity analysis of our choice in grid cell size showed no influence in the mechanics of headcut initiation. Model experiments began with a uniformly sloping floodplain with a 1 m deep trench that spanned the width of the domain located 450 m up-valley from the downstream boundary (Fig. 2A; Supplementary Fig. 1). We chose to use a trench instead of a meander cutoff to remove any potential dependencies on the shape of the meander cutoff. Results of our modeling experiments showed no dependency on the depth of the trench, hence through all model runs we held the trench depth constant. Additionally, we tested our model with meander cutoff segments and found no difference in the mechanics of headcut initiation. Across the model domain, we applied a randomly disturbed of ± 1 mm height to create realistic flow paths. We tested our choice in topographic roughness height, as well as simulations with no topographic roughness, and found that it did not influence the mechanics of headcut initiation. However, we found that simulations with a relatively large topographic roughness caused the roughness elements to steer the headcuts because the larger roughness elements strongly influenced flow paths.

Model simulations were run with two open boundaries, at the up-valley extent of the floodplain (upstream) and one at the down-valley extent of the floodplain (downstream). The upstream boundary condition was set to simulate a steady, uniform discharge carrying no

sediment and the downstream boundary condition is a fixed water level, set to maintain uniform flow depth over the floodplain. A computational time step of 12 seconds was used for all model simulations. The background horizontal eddy viscosity and diffusivity were set to be negligible at 1×10^{-4} m^2 s^{-1}. Model simulations used a morphological scale factor (MOR) of 10, which scales the morphology for each time step. Model results reported have been adjusted to account for the scaling factor. Additionally, we tested the sensitivity of our results to our choice in MOR and found no dependencies. All other parameters were left to the default values in Delft3D.

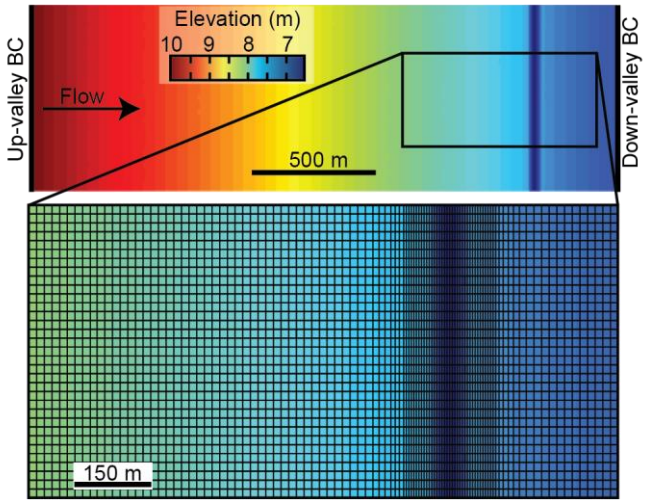

Supplementary Figure 1. Computational grid. *Topography data shown for T_w=90 m, $S=8\times10^{-4}$. The inset shows the topography data overlain with the computational grid. The grid has square cells, each 225 m^2, in the floodplain, and refines to rectangular grid cells of 75 m^2 at the trench.*

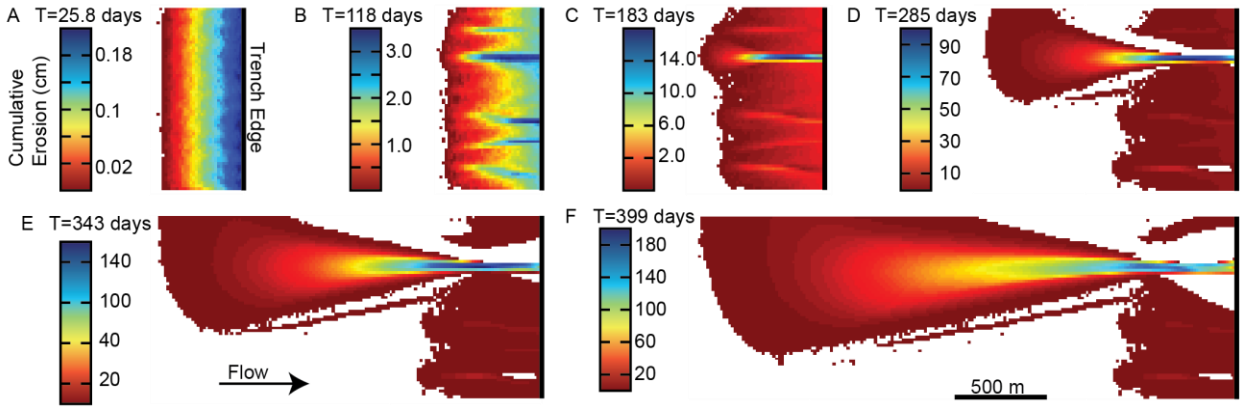

106

107 ***Supplementary Figure 2. Dynamics of headcut migration.*** *Maps of cumulative erosion show the*
108 *development and evolution of a headcut. Initially an erosional front develops (A) and headcuts are etched*
109 *into that front (B). Through time a dominant headcut arises (C) and migrates up-valley and broadens (D-*
110 *F). Model results shown are for* T_w*=90 m,* $S=8\times10^{-4}$*, and D=0.4 m.*

111

112

113

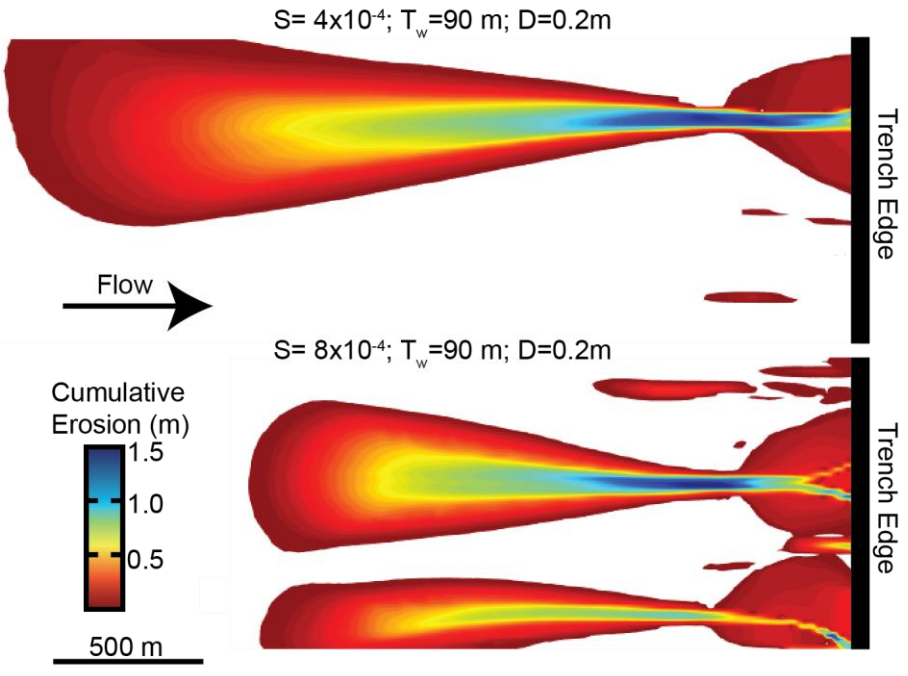

114

115 ***Supplementary Figure 3. Slope influence on headcutting.*** *Maps of cumulative erosion showing*
116 *increasing slope creating more stable headcuts, which migrate slower. Model results shown are for*
117 $S=4\times10^{-4}$*,* T_w*=90 m, and D=0.2 m (top) and* $S=8\times10^{-4}$*,* T_w*=90 m, and D=0.2 m (bottom).*

118

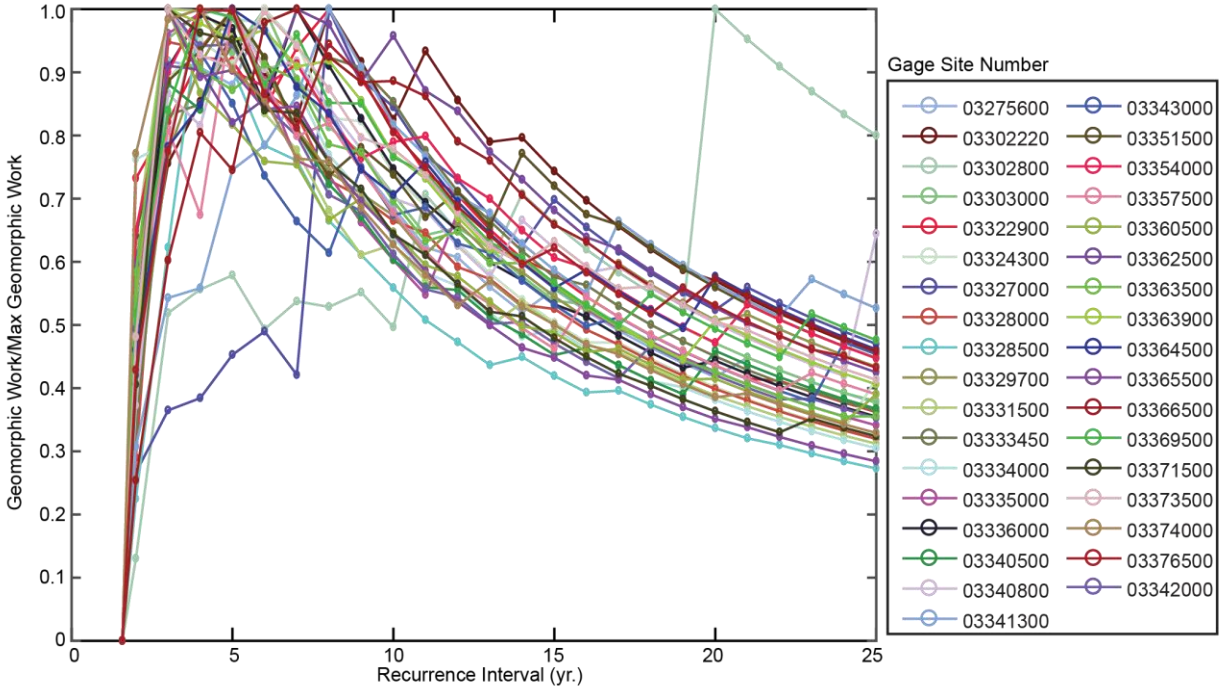

120

121 ***Supplementary Figure 4. Peak geomorphic work.*** *Plot showing peak geomorphic work as a*
122 *function of recurrence interval for 35 gages. Note most gaging stations' peak geomorphic work*
123 *occurs between a 3 and 8 year flood recurrence. Not shown on the plot is an outlier where*
124 *geomorphic work peaks at 40 years.*
125

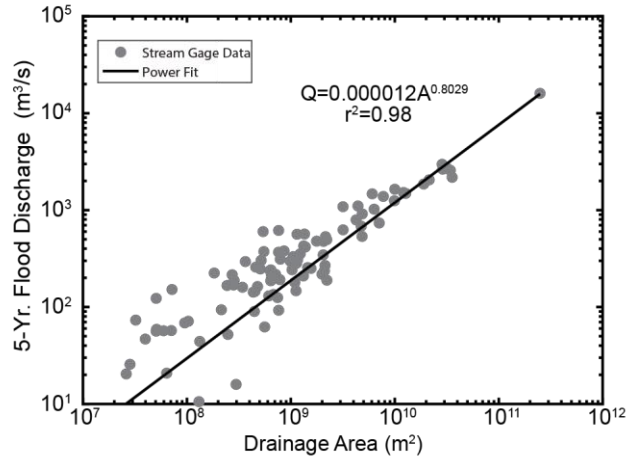

126

127 ***Supplementary Figure 5. Drainage area-discharge relationship.*** *Plot of 5 year flood discharge*
128 *as a function of drainage area. The black line is a power fit of the data used to convert all*
129 *mapped floodplains' drainage area to discharge.*
130

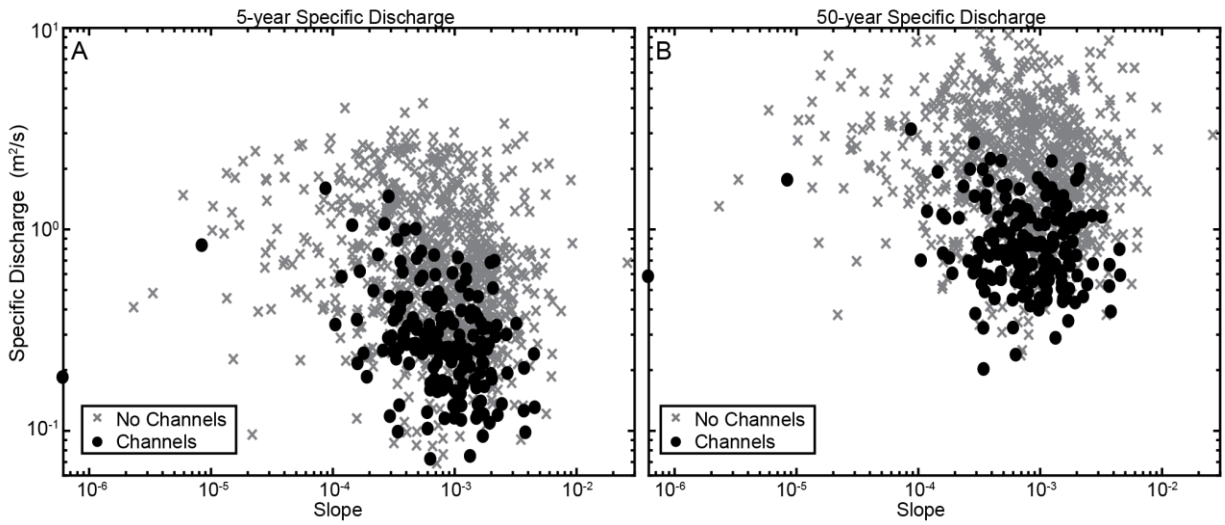

Supplementary Figure 6. Sensitivity analysis. *Sensitivity analysis of our choice in recurrence interval. (A) Specific discharge computed from a 5-year flood. (B) Specific discharge computed from a 50-year flood. Note that while the points shift in the y direction, the channelized floodplains (black dots) still cluster at lower specific discharges.*

REFERENCES

Bull, W.B., 1979, Threshold of critical power in streams: Geological Society of America Bulletin, v. 90, p.453-464, https://doi.org/10.1130/0016-7606(1979)90<453:TOCPIS>2.0.CO;2.

David, S.R., Edmonds, D.A. and Letsinger, S.L., 2017, Controls on the occurrence and prevalence of floodplain channels in meandering rivers: Earth Surface Processes and Landforms, v. 42, p. 460-472, https://doi.org/10.1002/esp.4002.

Nanson, G.C. and Croke, J.C., 1992, A genetic classification of floodplains: Geomorphology, v. 4, p. 459-486, https://doi.org/10.1016/0169-555X(92)90039-Q.

OpenTopography, 2013, *Indiana 2011-2013 statewide lidar data available*. La Jolla, CA: Univ. of California San Diego. http://www.opentopography.org/news/indiana-2011-2013-statewide-lidar-survey-data-available

Smith, M.J. and Cromley, R.G., 2012, Measuring historical coastal change using GIS and the change polygon approach: Transactions in GIS, v. 16, p. 3-15, https://doi.org/10.1111/j.1467-9671.2011.01292.x.

Wolman, M.G. and Miller, J.P., 1960, Magnitude and frequency of forces in geomorphic processes: The Journal of Geology, v. 68, p. 54-74.